Cellular/Molecular

Partial Mitochondrial Inhibition Causes Striatal Dopamine Release Suppression and Medium Spiny Neuron Depolarization via H_2O_2 Elevation, Not ATP Depletion

Li Bao, Marat V. Avshalumov, and Margaret E. Rice

Department of Physiology and Neuroscience and Department of Neurosurgery, New York University School of Medicine, New York, New York 10016

Mitochondrial dysfunction is a potential causal factor in Parkinson's disease. We show here that acute exposure to the mitochondrial complex I inhibitor rotenone (30–100 nM; 30 min) causes concentration-dependent suppression of single-pulse evoked dopamine (DA) release monitored in real time with carbon-fiber microelectrodes in guinea pig striatal slices, with no effect on DA content. Suppression of DA release was prevented by the sulfonylurea glibenclamide, implicating ATP-sensitive K^+ (K_{ATP}) channels; however, tissue ATP was unaltered. Because K_{ATP} channels can be activated by hydrogen peroxide (H_2O_2), as well as by low ATP, we examined the involvement of rotenone-enhanced H_2O_2 generation. Confirming an essential role for H_2O_2, the inhibition of DA release by rotenone was prevented by catalase, a peroxide-scavenging enzyme. Striatal H_2O_2 generation during rotenone exposure was examined in individual medium spiny neurons using fluorescence imaging with dichlorofluorescein (DCF). An increase in intracellular H_2O_2 levels followed a similar time course to that of DA release suppression and was accompanied by cell membrane depolarization, decreased input resistance, and increased excitability. Extracellular catalase markedly attenuated the increase in DCF fluorescence and prevented rotenone-induced effects on membrane properties; membrane changes were also largely prevented by flufenamic acid, a blocker of transient receptor potential (TRP) channels. Thus, partial mitochondrial inhibition can cause functional DA denervation via H_2O_2 and K_{ATP} channels, without DA or ATP depletion. Furthermore, amplified H_2O_2 levels and TRP channel activation in striatal spiny neurons indicate potential sources of damage in these cells. Overall, these novel factors could contribute to parkinsonian motor deficits and neuronal degeneration caused by mitochondrial dysfunction.

Key words: **basal ganglia; K_{ATP} channels; medium spiny neurons; mitochondria; Parkinson's disease; pesticide; rotenone**

Introduction

Parkinson's disease is a neurodegenerative disorder that selectively targets dopamine (DA) neurons of the substantia nigra pars compacta (SNc). Although the cause of degeneration of DA cells and their axonal projection to the striatum is not yet understood, postmortem samples from patients with Parkinson's disease show oxidative damage (Olanow and Tatton, 1999; Zhang et al., 2000), implicating a causal role for oxidative stress. Mitochondrial dysfunction has been implicated as an important source of this oxidative stress (Greenamyre et al., 2001; Orth and Schapira, 2002; Dauer and Przedborski, 2003; Dawson and Dawson, 2003; Fiskum et al., 2003). Key evidence includes decreased activity of mitochondrial complex I in the SNc and other tissues of Parkinson's disease patients (Parker et al., 1989; Schapira et al., 1990) and the recent discovery that mutation of a mitochondrial protein may underlie a familial form of early-onset Parkinson's disease (Valente et al., 2004). Moreover, partial inhibition of complex I in isolated mitochondria or synaptosomes causes increased production of reactive oxygen species (ROS), especially hydrogen peroxide (H_2O_2) (Votyakova and Reynolds, 2001; Fonck and Baudry, 2003; Sipos et al., 2003).

These observations have led to the development of a rodent model of Parkinson's disease based on chronic exposure to the mitochondrial complex I inhibitor, rotenone (Betarbet et al., 2000), which is a popular botanical pesticide that is harmless to plants, but toxic to insects, fish, and mammals (Dauer and Przedborski, 2003; Greenamyre et al., 2003). Strikingly, CNS damage in rotenone-treated rats occurs primarily in the basal ganglia and is accompanied by parkinsonian motor deficits (Ferrante et al., 1997; Betarbet et al., 2000; Höglinger et al., 2003; Sherer et al., 2003a; Fleming et al., 2004), as well as α-synuclein- and ubiquitin-containing inclusions that resemble cytopathological features of Parkinson's disease (Betarbet et al., 2000; Höglinger et al., 2003; Sherer et al., 2003a). Although chronic, low-level rotenone exposure can cause loss of DA axons in striatum with subsequent retrograde degeneration of DA neurons in the SNc (Betarbet et al., 2000; Sherer et al., 2003a; Alam and Schmidt, 2004), the losses are often minimal and accompanied by damage to

Received June 28, 2005; revised Sept. 12, 2005; accepted Sept. 20, 2005.

This work was supported by National Institutes of Health–National Institute of Neurological Disorders and Stroke Grant NS-36362 and by the National Parkinson Foundation. We are grateful to the Turner Biosystems Luminometer Grants Program for the grant of a TD-20/20 luminometer. We also appreciate advice on whole-cell recording from Drs. James M. Tepper and Abram Akopian.

Correspondence should be addressed to Dr. Margaret E. Rice, Department of Physiology and Neuroscience, New York University School of Medicine, 550 First Avenue, New York, NY 10016. E-mail: margaret.rice@nyu.edu.

DOI:10.1523/JNEUROSCI.2652-05.2005

 0270-6474/05/2510029-12$15.00/0

other cells, including striatal medium spiny neurons (Ferrante et al., 1997; Höglinger et al., 2003; Fleming et al., 2004).

In most animal models of Parkinson's disease, >80% DA neuron loss is typically required to produce motor symptoms (Zigmond et al., 1990), which raises the question of how rotenone produces parkinsonian motor deficits with limited loss of nigrostriatal DA neurons. This paradox has led to the proposal that rotenone-induced motor deficits result from multisystem degeneration (Höglinger et al., 2003). In contrast, recent studies indicate that these deficits can be reversed by the DA precursor L-dihydroxyphenylalanine (L-DOPA) (Alam and Schmidt, 2004), confirming that they are indeed DA dependent. Together, these findings suggest that rotenone might cause a functional rather than anatomical loss of DA transmission. Here, we show that rotenone causes dynamic suppression of DA release from axon terminals in the striatum as a consequence of H_2O_2 generation and activation of ATP-sensitive K^+ (K_{ATP}) channels.

Materials and Methods

Brain slice preparation. All animal handing procedures were in accordance with National Institutes of Health guidelines and were approved by the New York University School of Medicine Animal Care and Use Committee. The procedure for preparing coronal slices of striatum was similar to that described previously (Koós and Tepper, 1999). Young adult guinea pigs (male Hartley; 150–250 g) were deeply anesthetized with 40 mg/kg pentobarbital (i.p.) and perfused transcardially with ~30 ml of nearly frozen (~0°C) modified artificial CSF (ACSF) at a rate of ~10 ml/min. The physiological saline used for perfusion and for preparing slices for whole-cell recording contained the following (in mM): 225 sucrose, 2.5 KCl, 0.5 $CaCl_2$, 7 $MgCl_2$, 28 $NaHCO_3$, 1.25 NaH_2P0_4, 7 glucose, 1 ascorbate, and 3 pyruvate (Koós and Tepper, 1999). After perfusion, the brain was removed into this ice-cold solution for 1–2 min and then bisected, and one hemisphere was blocked and fixed to the stage of a Vibratome (Ted Pella, St. Louis, MO) for slice preparation. For voltammetric recording and determination of DA, dihydroxyphenylacetic acid (DOPAC), and ATP contents, slices (400 μm thickness) were normally cut in ice-cold HEPES-buffered ACSF containing (in mM) 120 NaCl, 20 $NaHCO_3$, 10 glucose, 6.7 HEPES acid, 5 KCl, 3.3 HEPES sodium salt, 2 $CaCl_2$, and 2 $MgSO_4$, saturated with 95% O_2/5% CO_2, and maintained in this medium at room temperature for at least 1 h after cutting (Chen and Rice, 2001; Avshalumov and Rice, 2003; Avshalumov et al., 2003). For imaging and whole-cell recording, slices (300 μm thickness) were initially transferred to a chamber maintained at 34°C for 30 min in a solution containing the following (in mM): 125 NaCl, 2.5 KCl, 2 $CaCl_2$, 1 $MgCl_2$, 25 $NaHCO_3$, 1.25 NaH_2PO_4, 25 glucose, 1 ascorbate, and 3 pyruvate, pH 7.3–7.4, equilibrated with 95% O_2/5% CO_2. The chamber was then allowed to cool to room temperature during an additional period of at least 30 min before recording. In some experiments, the effect of rotenone on evoked DA release was examined in slices prepared and maintained for whole-cell recording; results were indistinguishable between slice preparations such that data from both were pooled in reported averages. All experiments were conducted at 32°C in submerged slices superfused at 1.2 ml/min with recording ACSF containing the following (in mM): 124 NaCl, 3.7 KCl, 26 $NaHCO_3$, 2.4 $CaCl_2$, 1.3 $MgSO_4$, 1.3 KH_2PO_4, and 10 glucose, equilibrated with 95% O_2/5% CO_2.

Voltammetric recording. Axon-terminal DA release was elicited in dorsolateral striatum using a bipolar stimulating electrode placed on the slice surface and detected at a carbon fiber microelectrode positioned ~100 μm dorsal to the bipolar electrode (Chen and Rice, 2001; Avshalumov et al., 2003). The stimulus was either a single pulse or a 30 pulse train at 10 Hz; the pulse duration was 100 μs. Stimulus intensity (0.6–0.9 mA) was perimaximal for single-pulse evoked release (Cragg, 2003; Rice and Cragg, 2004). Under these conditions, DA release is tetrodotoxin sensitive and Ca^{2+} dependent (Chen and Rice, 2001). Evoked DA release was monitored using fast-scan cyclic voltammetry (Millar Voltammeter; Dr. Julian Millar, Queen Mary, University of London, London, UK) with 8 μm carbon fiber microelectrodes (2–4 μm tips) (MPB Electrodes, London, UK; or WPI, Sarasota, FL). Scan rate was 800 V/s, voltage range was −0.7 to +1.3 V versus Ag/AgCl, and sampling interval was 100 ms. Data acquisition and analysis were as described previously (Chen and Rice, 2001). Released DA was identified by characteristic oxidation and reduction peak potentials (see Fig. 1*A*); extracellular DA concentration ($[DA]_o$) was calculated from postexperimental electrode calibration in the recording chamber at 32°C in all media used in a given experiment (e.g., ACSF and ACSF plus rotenone).

HPLC analysis of tissue DA and DOPAC contents. In separate experiments, striatal DA and DOPAC contents were determined in slices exposed to 50 nM rotenone for 30 min; the paired control for each sample was from the contralateral striatum maintained in ACSF in the recording chamber under otherwise-identical conditions. Incubation conditions paralleled those for voltammetric recording studies, with 60 min in the recording chamber in ACSF at 32°C (corresponding to 30 min equilibration plus 30 min control recording), followed by 30 min exposure to rotenone or continued incubation in ACSF alone. After incubation, excess solution was carefully removed from a given slice and a sample of dorsal striatum (3–10 mg) was taken, weighed, frozen on dry ice, and then stored at −80°C until analysis. On the day of analysis, samples were diluted 1:10 with ice-cold, deoxygenated HPLC eluent, sonicated, and spun in a microcentrifuge for 2 min at 14,000 × *g*, and the supernatant was injected directly into the HPLC system as described previously (Chen et al., 2001). The mobile phase was 50 mM NaH_2PO_4, with 3 m/L sodium octylsulfate, 23.2 mg/L heptanesulfonic acid, 8 mg/L EDTA, and 10% methanol, pH 3 (Witkovsky et al., 1993); the electrochemical detector was a glassy carbon electrode set at +0.7 V versus Ag/AgCl. Tissue DA and DOPAC content data are given as micromoles per gram tissue wet weight (micromoles per gram).

Determination of striatal ATP content. Striatal ATP content in incubated brain slices was determined in separate experiments using a TD-20/20 Luminometer (Turner Biosystems, Sunnyvale, CA) with an Enlighten ATP assay kit (Promega, Madison, WI). This method is based on the luciferase-catalyzed reaction of ATP with luciferin with light emission at 560 nm. Pilot experiments indicated that tissue ATP content was lower in frozen tissue samples than in unfrozen tissue, so that in all subsequent studies ATP content was determined in unfrozen tissue samples immediately after incubation. Test slices were superfused with ACSF at 32°C in the recording chamber for 60 min, and then with 50 nM rotenone for an additional 5, 10, 20, or 30 min or with 100 nM rotenone or ACSF containing 1 mM glucose for 30 min; paired control slices from the contralateral striatum were maintained in normal ACSF for the same time periods as test slices. After incubation, samples of dorsal striatum (3–8 mg) were weighed in microcentrifuge vials and then sonicated immediately in 5% trichloracetic acid (100-fold dilution; i.e., 99 μl/mg tissue) to stop ATP degradation. Sonicated samples were centrifuged for 2 min at 14,000 × *g*; the supernatant was diluted 1000-fold in PBS, pH 7.75, and then mixed with assay kit reagents according to the manufacturer's instructions. Tissue ATP content (micromoles per gram of tissue wet weight) was determined from standard curves prepared immediately before each analysis; similar curves were obtained with ATP standards prepared from stock solutions included in the Enlighten kit and from stock solutions made in-house using commercially available ATP (Sigma, St. Louis, MO).

Visualized whole-cell recording. Striatal cells were visualized under infrared differential interference contrast microscopy using an Olympus BX51WI fixed-stage microscope (New York/New Jersey Scientific, Middlebush, NJ) with a 40× water immersion objective; a Pro-Scan 11 *z*-axis controller (Prior Scientific, Rockland, MA) was used to sharpen focus for fluorescence imaging. Whole-cell recordings were obtained with patch pipettes pulled from 1.5/0.86 mm outer/inner diameter borosilicate glass (Sutter Instrument, Novato, CA) on a Flaming/Brown model P-97 puller (Sutter Instrument). Pipettes had open tip diameters of <2 μm and resistances of 5–7 MΩ. The intracellular solution contained the following (in mM): 120 K-gluconate, 20 KCl, 2 MgCl, 10 Na-HEPES, 10 EGTA, 3 Na_2-ATP, 0.2 GTP, pH adjusted to 7.2–7.3 with KOH, 280–290 mOsm (Koós and Tepper, 1999). This backfill solution also contained Alexa Red (0.1%) for cell visualization and 2′,7′-

dihydrodichloro-fluorescein (H_2DCF) diacetate (H_2DCFDA) (7 μM) for H_2O_2 imaging (Avshalumov et al., 2005).

Cell input resistance was calculated from the current–voltage plot of a family of hyperpolarizing and depolarizing current pulses; measurements were taken 300 ms after pulse onset at the same membrane potential (−90 mV) for each neuron under control and experimental conditions (Nisenbaum and Wilson, 1995). In some experiments, the time course of rotenone-induced changes in input resistance was determined from current injection pulses (−0.1 nA; 1 s) applied under control conditions and throughout rotenone application. Whole-cell recording data were acquired using an Axopatch 200B amplifier and Digidata board 1322A controlled by Clampex 9.0 (Molecular Devices, Union City, CA), with ClampFit software (Molecular Devices) used for data analysis; recordings were corrected for a liquid junction potential using a value of 7.2 mV calculated using Clampex.

H_2O_2 imaging. To image intracellular ROS, H_2DCFDA was loaded into individual medium spiny neurons via the patch pipette used for simultaneous physiological recording. This peroxide-selective dye is cleaved by intracellular esterases to form H_2DCF, which becomes fluorescent dichlorofluorescein (DCF) after oxidation by H_2O_2 or other ROS (Reynolds and Hastings, 1995; Sah and Schwartz-Bloom, 1999). Once whole-cell configuration was obtained, cell physiology was monitored for ~20 min to allow sufficient time for diffusion of the dye into the cell. Data were acquired using a Cascade CCD camera (Roper Scientific, Tucson, AZ) and an illuminator and monochrometer from Photon Technology International (Lawrenceville, NJ) and were analyzed using Image Master software version 1.5 (Photon Technology International). The excitation wavelength used for DCF was 488 nm with fluorescence emission at 535 nm. To minimize DCF photooxidation, illumination was limited to 800 ms exposures at 1.2 s intervals with two-frame averaging. A background image was taken before H_2DCFDA infiltrated a given cell; in subsequent analysis, this background image was subtracted from each averaged image for that cell. Fluorescence intensity for 535 nm emission in these background-subtracted frame averages was normalized; average data are presented as follows: [(intensity − basal)/(basal)] × 100%.

Chemicals and statistical analysis. Rotenone, glibenclamide, tolbutamide, flufenamic acid, tetrodotoxin (TTX), and dimethylsulfoxide (DMSO), as well as components of ACSF and the intracellular recording solution were from Sigma. Catalase (bovine liver) was from Calbiochem (La Jolla, CA). Alexa Red and H_2DCFDA were from Invitrogen (Eugene, OR). Individual stock solutions of rotenone, glibenclamide, flufenamic acid, and H_2DCFDA, were made in DMSO to yield a final DMSO level of 0.01% in ACSF or in the recording pipette. Control data for these agents were obtained in 0.01% DMSO in appropriate media, which had no effect on any measured parameter.

Data are given as means ± SE; n = number of slices for DA release, ATP, DA, and DOPAC content data and number of cells for electrophysiology and imaging data. Statistical analyses of these data were performed using paired or unpaired Student's t test as appropriate, with one-way ANOVA with Dunnett's *post hoc* analysis used to evaluate progressive changes in evoked $[DA]_o$, DCF fluorescence intensity, or medium spiny neuron membrane properties during rotenone exposure versus control; differences were considered significant for $p < 0.05$. For voltammetric recording, at least three consistent control records were obtained before drug or enzyme application. In studies with rotenone, exposure time was usually limited to 30 min.

Results

Suppression of single-pulse evoked $[DA]_o$ by nanomolar rotenone

Local stimulation in the striatum elicits the release of DA, as well as other transmitters, including glutamate. We have previously shown that concomitantly released glutamate acting at AMPA receptors (AMPARs) can inhibit axonal DA release via generation of H_2O_2 and subsequent opening of K_{ATP} channels (Avshalumov and Rice, 2003; Avshalumov et al., 2003). To reveal glutamate-dependent regulation of DA release requires multiple-pulse stimulation, in which initial pulses produce modulatory H_2O_2 that inhibits DA release evoked by subsequent pulses. When a single stimulus pulse is used, however, DA release is free from indirect modulation by AMPAR activation and endogenously generated H_2O_2 (Avshalumov et al., 2003).

In the present studies, therefore, we initially examined the effect of rotenone on single-pulse evoked DA release (Fig. 1*A*) to avoid confounding effects from glutamate release. Under control conditions, average single-pulse evoked $[DA]_o$ was 1.09 ± 0.04 μM ($n = 32$), which was stable for at least 2 h when elicited at stimulation intervals of either 2.5 or 5 min (data not shown). When slices were subsequently exposed to 50 nM rotenone, which is near the IC_{50} for mitochondrial complex I inhibition (Betarbet et al., 2000; Votyakova and Reynolds, 2001), this mitochondrial inhibitor caused an immediate decrease in evoked $[DA]_o$ that reached significance within 5 min of rotenone superfusion ($p < 0.05$; $n = 10$) (Fig. 1*B*). Evoked $[DA]_o$ decreased progressively during continued rotenone exposure, with an average decrease of 32 ± 3% versus same-site control ($p < 0.01$; $n = 10$) after 30 min in rotenone (Fig. 1*B*). We then examined the concentration dependence of rotenone-induced DA release suppression for 30 nM to 1 μM rotenone; 30 nM was of interest because this is the concentration that Betarbet et al. (2000) estimated is maintained in the brain in their studies of chronic low-dose rotenone exposure *in vivo*. The initial response to 30 nM ($n = 6$) or 100 nM ($n = 6$) rotenone was similar to that seen with 50 nM; however, concentration-dependent release suppression was seen after 25 min in rotenone, with a significant difference in evoked $[DA]_o$ between 30 nM and 50 or 100 nM and between 50 and 100 nM ($p < 0.01$ for each comparison; ANOVA) (Fig. 1*C*). Higher rotenone concentrations (500 nM to 1 μM) caused complete loss of evoked DA release within minutes of exposure (data not shown); release suppression was irreversible for all concentrations of rotenone tested. Further mechanistic studies were conducted using 50 nM rotenone.

Analysis of tissue DA content using HPLC showed that DA levels in dorsal striatum were unaltered by acute, low-level rotenone exposure (50 nM; 30 min), with 0.43 ± 0.04 μmol/g tissue wet weight in control slices and 0.42 ± 0.06 μmol/g in paired slices after rotenone exposure ($p > 0.05$; $n = 6$ slice pairs). In the same slices, DOPAC content was 0.042 ± 0.001 μmol/g in controls and 0.042 ± 0.006 μmol/g after rotenone ($p > 0.05$). Maintained DA and DOPAC contents indicate that decreased evoked $[DA]_o$ in the presence of rotenone was not attributable to depletion of the releasable pool of DA and that release suppression was not accompanied by profound changes in DA turnover within this time frame.

DA release suppression by rotenone requires K_{ATP} channels but not a decrease in ATP

Given that DA release can be inhibited by K_{ATP} channel opening (Avshalumov and Rice, 2003) and that rotenone, as a mitochondrial inhibitor, can cause a decrease in ATP (Davey and Clark, 1996; Fonck and Baudry, 2003; Sherer et al., 2003b), we examined whether the effect of rotenone on evoked $[DA]_o$ involved K_{ATP} channels using the selective K_{ATP} channel blocker glibenclamide (3 μM) (Avshalumov and Rice, 2003; Avshalumov et al., 2005). In contrast to the enhancement in pulse-train evoked $[DA]_o$ seen when K_{ATP} channels are blocked in striatal slices (Avshalumov and Rice, 2003; Avshalumov et al., 2003), glibenclamide (3 μM) had no effect on single-pulse evoked $[DA]_o$, indicating the absence of basal K_{ATP} channel regulation of DA under control conditions (data not shown). In the continued presence of glibenclamide, however, the usual rotenone-induced suppression of

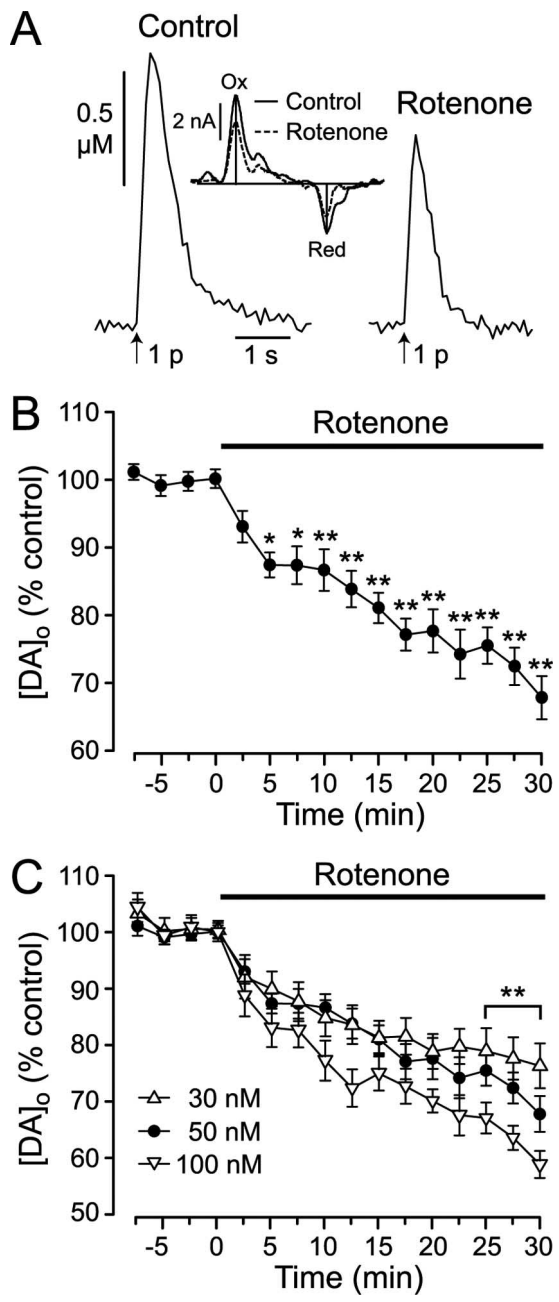

Figure 1. Rotenone causes suppression of axonal DA release in dorsal striatum. ***A***, Representative DA release records elicited by a single stimulus pulse under control conditions and after 30 min exposure to rotenone (50 nM) at the same recording site. Inset, Cyclic voltammograms taken at the maximum $[DA]_o$ for each record; dopamine was identified by characteristic oxidation (Ox) and reduction (Red) peak potentials (typically +600 and −200 mV vs Ag/AgCl). ***B***, Time course of rotenone-induced suppression of single-pulse evoked $[DA]_o$ elicited at 2.5 min intervals throughout rotenone exposure ($n = 10$; $^*p < 0.05$; $^{**}p < 0.01$ rotenone vs control; ANOVA). ***C***, Concentration dependence of rotenone-induced suppression of single-pulse evoked DA release. Release suppression induced by rotenone at 30 nM ($n = 6$), 50 nM ($n = 10$), or 100 nM ($n = 6$) differed significantly at the time points indicated ($n = 6$; $^{**}p < 0.01$). Error bars indicate SE.

evoked $[DA]_o$ was completely prevented ($p > 0.05$; $n = 5$) (Fig. 2*A*,*B*). Because glibenclamide can have nonspecific effects, albeit at higher concentrations than that tested here (Crepel et al., 1993; Schaffer et al., 1999), we also examined the effect of 100 nM glibenclamide, which is specific for K_{ATP} channels (Liss et al., 1999). In 100 nM glibenclamide, rotenone-induced suppression of evoked $[DA]_o$ was also prevented (1.18 ± 0.08 μM in glibenclamide alone and 1.10 ± 0.08 μM after 30 min in 50 nM rotenone in the continued presence of glibenclamide; $p > 0.05$; $n = 5$), although a longer exposure to 100 nM glibenclamide was required to inhibit the effect of rotenone (45 vs 30 min for 3 μM glibenclamide). We then tested a second K_{ATP} channel blocker, tolbutamide (200 μM) (Avshalumov and Rice, 2003). As with glibenclamide, single-pulse evoked $[DA]_o$ was not altered by tolbutamide; however, this sulfonylurea, too, prevented DA release suppression by 50 nM rotenone ($p > 0.05$ vs tolbutamide alone; $n = 3$) (Fig. 2*C*,*D*). Together, these data demonstrate that K_{ATP} channel opening was required for the effect of rotenone on DA release.

We then determined the ATP content of striatal slices maintained in the recording chamber under control conditions and after exposure to rotenone (50 nM) for 5, 10, 20, or 30 min. The average ATP content of control slices prepared as usual and then maintained in the recording chamber for 1 h at 32°C was 1.26 ± 0.04 μmol/g tissue wet weight ($n = 10$). Assuming that ATP is localized primarily within the intracellular compartment, this would represent an average intracellular concentration of ~1.8 mM (1 g of tissue ≈ 1 ml), based on an intracellular volume fraction of 0.59 estimated from the extracellular volume fraction in striatum of 0.21 (Rice and Nicholson, 1991) and the usual fraction of brain solids in forebrain tissue of 0.20 (Rice and Russo-Menna, 1998). The ATP contents of slices maintained under control conditions for an additional period of 5–30 min were unchanged from those in 1 h controls ($p > 0.05$ for 1 vs 1.5 h; $n =$ 10–12 slices per condition). Strikingly, ATP content was unaltered by exposure to 50 nM rotenone during comparable time periods, with no difference in ATP content versus paired control at any time point examined ($p > 0.05$; $n = 10$–12 slice pairs) (Fig. 3). Given the greater effect of 100 nM rotenone on evoked $[DA]_o$ after 30 min exposure, we also determined the effect of this higher rotenone concentration on ATP content at this single time point versus that in paired control slices. In contrast to the minimal effect of 50 nM rotenone, 30 min exposure to 100 nM rotenone caused a significant decrease in ATP content of 14 ± 3% ($p < 0.01$ vs paired control; $n = 11$ slice pairs) (data not shown).

Although 50 nM rotenone did not cause a significant change in ATP, the tendency toward a decrease after 30 min (~95% of paired control; $p > 0.05$ vs control; $n = 12$) (Fig. 3) suggested that subtle alteration in ATP levels might contribute to K_{ATP} channel opening and suppression of DA release with this concentration of rotenone. To test this hypothesis, we induced ATP depletion in striatal slices by decreasing the glucose concentration of the superfusing ACSF to 1 mM, and then examined the consequences of this depletion on single-pulse evoked DA release. After 1 h in the chamber in normal ACSF (10 mM glucose), slices were either maintained for an additional 30 min in normal ACSF, or the superfusion solution was changed to ACSF with 1 mM glucose for 30 min. After 30 min in low glucose, striatal ATP content fell by a significant 14%, from 1.22 ± 0.05 μmol/g in control slices to 1.05 ± 0.04 μmol/g in low glucose ($p < 0.001$ vs control; $n = 13$ slice pairs) (Fig. 4*A*). In companion experiments, slices were equilibrated in the chamber for 30 min in normal ACSF, and then single-pulse evoked DA release was monitored at 5 min intervals; after 30 min of control recording in normal ACSF, the solution was changed to ACSF with 1 mM glucose for an additional 30 min, followed by washout with normal ACSF. Despite the significant decrease in tissue ATP content after 30 min in low glucose, evoked $[DA]_o$ was unaltered ($p > 0.05$ for low glucose vs either control or wash; $n = 5$) (Fig. 4*B*,*C*). These data indicate that a

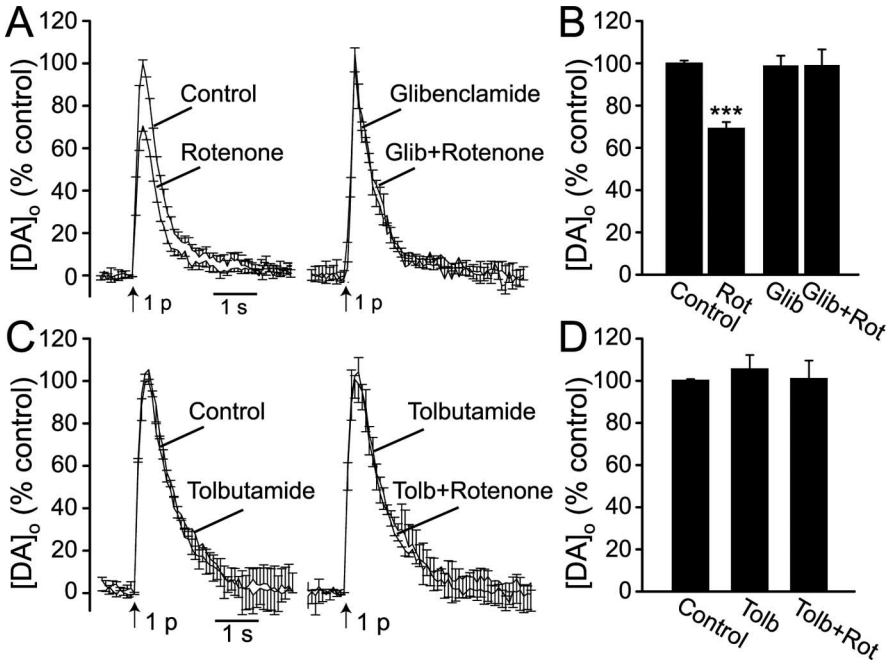

Figure 2. Rotenone-induced suppression of DA release requires K_{ATP} channel opening. ***A***, Average DA release records after single-pulse stimulation elicited at 5 min intervals under control conditions and after 30 min exposure to rotenone (50 nM; $n = 7$) compared with release in the presence of glibenclamide (Glib) (3 μM) and glibenclamide plus rotenone ($n = 5$). Data are normalized, with maximum evoked $[DA]_o$ under control conditions for each slice taken as 100%. ***B***, Rotenone (Rot) causes a decrease in evoked $[DA]_o$ (***$p < 0.001$ vs control; $n = 7$). Glibenclamide had no effect on single-pulse evoked DA release; however, this K_{ATP} channel blocker completely prevented the usual suppression of DA release in the presence of rotenone ($n = 5$; $p > 0.05$ vs glibenclamide alone). ***C***, Average single-pulse evoked $[DA]_o$ under control conditions, in the presence of tolbutamide (Tolb) (200 μM), and after 30 min exposure to rotenone (50 nM) in the presence of tolbutamide ($n = 3$). ***D***, Tolbutamide had no effect on single-pulse evoked DA release; however, it completely prevented DA release suppression by rotenone ($n = 3$; $p > 0.05$ vs tolbutamide alone). Error bars indicate SE.

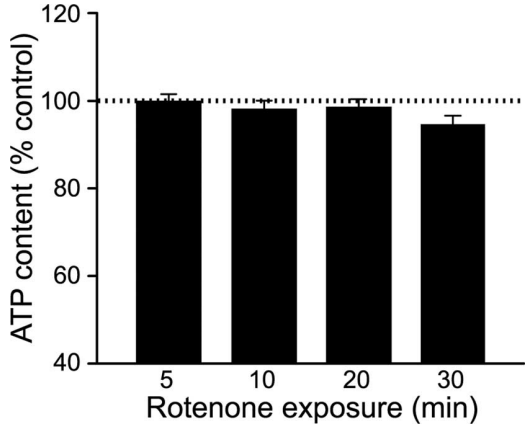

Figure 3. Acute rotenone exposure does not alter striatal ATP content. Average ATP content in dorsal striatum from striatal slices exposed to rotenone (50 nM) for 5, 10, 20, or 30 min. Data are given as percentage control (% control), with the ATP content of paired slices incubated for the same duration in ACSF alone taken as 100%. Tissue ATP content did not differ between rotenone-exposed and control slices at any time point ($p > 0.05$ vs paired control; $n = 10–12$). Error bars indicate SE.

<15% decrease in tissue ATP content alone would be unlikely to contribute to DA release suppression.

Rotenone-induced DA release suppression requires generation of H_2O_2

Another consequence of partial mitochondrial complex I inhibition by rotenone is enhanced production of H_2O_2, demonstrated previously in studies with isolated mitochondria (Kwong and Sohal, 1998; Votyakova and Reynolds, 2001; Gyulkhandanyan and Pennefather, 2004; Kudin et al., 2004) or synaptosomes (Sipos et al., 2003). Given that increased levels of endogenously generated H_2O_2 can cause K_{ATP} channel opening (Avshalumov and Rice, 2003; Avshalumov et al., 2003, 2005), we tested whether inhibition of axonal DA release by rotenone involved H_2O_2 using an H_2O_2-metabolizing enzyme, catalase (500 U/ml). Implicating a key role for H_2O_2, the effect of 50 nM rotenone on single-pulse evoked $[DA]_o$ was completely prevented by catalase ($p > 0.05$ vs same-site control; $n = 5$) (Fig. 5*A*,*B*). Heat-inactivated catalase (Avshalumov et al., 2003) did not alter rotenone-induced suppression of DA release ($n = 2$); these data are included in control averages.

As discussed above, local stimulation elicits the release not only of DA, but also other endogenous transmitters, including glutamate. In dorsal striatum, concurrent glutamate release during pulse-train stimulation leads to AMPAR-dependent generation of H_2O_2 and consequent suppression of DA release via K_{ATP} channel opening (Avshalumov et al., 2003). We therefore examined whether the effects of rotenone on evoked $[DA]_o$ persisted under conditions that normally produce H_2O_2, e.g., pulse-train stimulation (30 pulses at 10 Hz). With this stimulation paradigm (applied at 10 min intervals), average peak $[DA]_o$ was 1.09 ± 0.07 μM ($n = 14$). Suppression of axonal DA release by rotenone not only persisted under these conditions but was, in fact, amplified. The average decrease after 30 min in 50 nM rotenone was $41 \pm 3\%$ ($p < 0.001$ vs same-site control; $n = 7$), which was significantly greater than that seen with single-pulse evoked DA release under the same conditions ($p < 0.05$ pulse-train vs single-pulse stimulation). A significant role for rotenone-induced H_2O_2 generation was again indicated by the complete prevention of DA release suppression when rotenone was applied in the presence of catalase (500 U/ml) ($p > 0.05$ rotenone vs same-site control; $n = 5$) (Fig. 6*B*); rotenone-induced release suppression again persisted in heat-inactivation catalase ($n = 2$); these data were included in control pulse-train averages. As described previously (Avshalumov and Rice, 2003), pulse-train evoked release was enhanced in the presence of glibenclamide (3 μM) ($n = 5$; $p < 0.001$ glibenclamide vs control), indicating K_{ATP} channel activation (via AMPAR-dependent H_2O_2 generation) during local pulse-train stimulation (Avshalumov and Rice, 2003). In the continued presence of glibenclamide, the effect of rotenone on pulse-train evoked DA release was completely prevented ($n = 5$; $p > 0.05$ glibenclamide vs rotenone) (Fig. 6*C*).

Rotenone-induced H_2O_2 generation and physiological effects in medium spiny neurons

Although selective detection of H_2O_2 generation in DA axons is not possible at the present time, a window onto striatal H_2O_2 generation can be provided by monitoring H_2O_2-sensitive DCF

fluorescence in individual neurons after introduction of H_2DCFDA into cells via a patch pipette (Avshalumov et al., 2005). We therefore examined H_2O_2 generation in medium spiny neurons, which are the predominant neuronal cell type in the striatum (Kemp and Powell, 1971). Medium spiny neurons were identified by their characteristic morphology (Fig. 7) and electrophysiological characteristics (Fig. 8), as described previously (Nisenbaum and Wilson, 1995; Koós and Tepper, 1999). Basal DCF fluorescence was detected in all recorded medium spiny neurons ($n = 13$), indicating tonic generation of H_2O_2 and/or other ROS (Fig. 7*B*). Intracellular H_2O_2 levels began to rise within minutes of exposure to 50 nM rotenone (Fig. 7*A*,*B*), with a significant increase detected after 4 min of rotenone exposure ($p < 0.001$; $n = 13$) (Fig. 7*B*). After 5–7 min exposure to rotenone, the increase in DCF fluorescence reached a plateau that was maintained throughout the usual 30 min monitoring period, with an average increase of 58 ± 5% above basal levels ($p < 0.001$; $n = 13$) (Fig. 7*C*). This plateau did not reflect dye saturation, because an additional increase in fluorescence intensity could be induced by application of exogenous H_2O_2 (1.5 mM) (data not shown); however, whether it indicated a constant level of H_2O_2 generation or was an artifact of the irreversible DCF activation by H_2O_2 (Avshalumov et al., 2005) cannot be discerned with currently available methods.

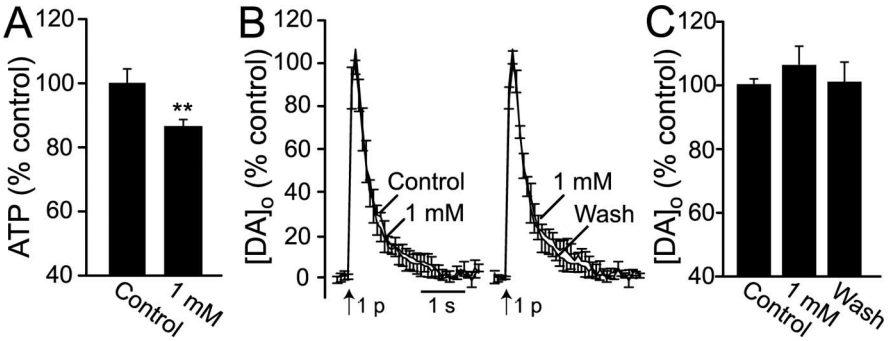

Figure 4. Evoked DA release is unaltered by a drop in ATP caused by low glucose. ***A***, ATP content in dorsal striatum from slices maintained in the recording chamber in normal ACSF with 10 mM glucose (Control) and/or in modified ACSF with low glucose (1 mM) for 30 min, given as percentage control (% control). Incubation in low glucose caused a significant decrease in striatal ATP content (***$p < 0.001$ vs paired control; $n = 13$). ***B***, Average DA concentration–time profiles in dorsal striatum after single-pulse stimulation elicited at 5 min intervals in normal ACSF, after 30 min in ACSF with 1 mM glucose, and after 30 min washout with normal ACSF (Wash) ($n = 5$). ***C***, Maximum evoked $[DA]_o$ did not differ between 1 mM and 10 mM glucose-containing ACSF ($n = 5$; $p > 0.05$, 1 mM vs either control or wash). Error bars indicate SE.

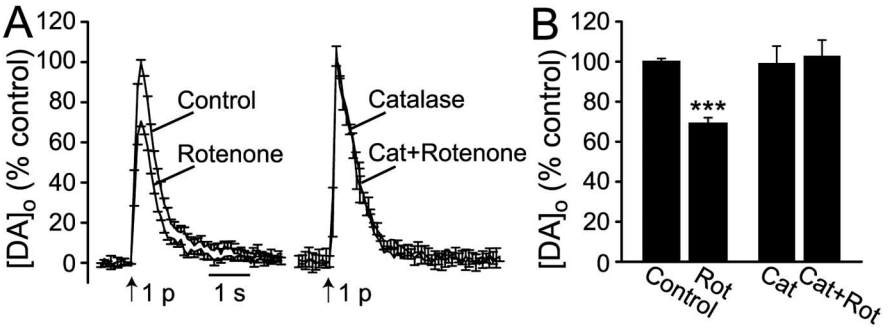

Figure 5. Rotenone-induced suppression of DA release requires H_2O_2. ***A***, Average DA release records elicited by single-pulse stimulation under control conditions (Control) and after 30 min exposure to rotenone (Rot) (50 nM) compared with the effect of rotenone on single-pulse release in the presence of catalase (Cat) (500 U/ml). ***B***, Under control conditions (ACSF alone or ACSF plus heat-inactivated catalase), rotenone caused a significant decrease in peak evoked $[DA]_o$ (***$p < 0.001$, rotenone vs control; $n = 9$); however, this effect of rotenone was prevented in the continued presence of catalase ($p > 0.05$ vs same-site control in catalase alone; $n = 5$). Error bars indicate SE.

The electrophysiological characteristics of these cells confirmed their identity as medium spiny neurons (Fig. 8). These cells had a mean resting potential of 79.5 ± 5 mV and input resistance of 83 ± 7 MΩ ($n = 13$); they were not spontaneously active *in vitro*, but showed spike activity with depolarizing current injection (Fig. 8*A*). Rotenone (50 nM) caused membrane depolarization from −79.5 ± 5 to −70.2 ± 2.1 mV ($p < 0.01$; $n = 13$), an increase in spike frequency with depolarizing current injection (3.3 ± 0.7 vs 11.8 ± 1.1 Hz; $p < 0.01$; $n = 13$) (Fig. 8*B*), and a decrease in input resistance (83 ± 7 vs 47 ± 8.6 MΩ; $p < 0.05$; $n = 13$).

To examine whether H_2O_2 contributed to the physiological consequences of rotenone exposure, we applied rotenone in the presence of catalase (500 U/ml). Catalase markedly attenuated the increase in DCF fluorescence induced by 50 nM rotenone (data not shown), implying that increases in intracellular H_2O_2 levels in a given cell reflects contributions from surrounding cellular elements, as well as its own mitochondria. This observation also suggests that H_2O_2 was the predominant ROS detected by DCF fluorescence. Catalase alone had no effect on medium spiny neuron membrane properties (Fig. 8*C*); however, the continued presence of catalase completely prevented the consequences of rotenone on the physiological properties of medium spiny neurons ($n = 3$) (Fig. 8*D*). In control experiments, heat-inactivated catalase had no effect on resting cell membrane properties, nor on the usual increase in DCF fluorescence and cell excitability seen during rotenone exposure ($n = 3$). Prevention of these responses by active catalase demonstrates that rotenone-induced membrane depolarization and increased excitability in medium spiny neurons were H_2O_2 dependent.

We then evaluated the time course of rotenone-induced changes in membrane potential and input resistance in medium spiny neurons for comparison with those of DA release suppression and H_2O_2 generation. Continuous current-clamp recording indicated that membrane depolarization began within minutes of exposure to rotenone (50 nM) (Fig. 9*A*), with a progressive change in membrane potential that differed significantly from control after 4 min in rotenone ($p < 0.05$ vs same cell-control; $n = 10$), and then reached a plateau after ~7 min ($p < 0.01$; $n = 10$). Rotenone-induced changes in input resistance in these cells showed a similar time course, with a decrease in resistance (i.e., an increase in conductance, indicative of channel opening) that reached significance after 5 min, with a subsequent plateau ($p < 0.01$ vs same cell-control; $n = 10$).

Previous studies have shown that striatal medium spiny neurons respond to conditions of metabolic stress with depolarization that is mediated by nonselective cation channels (Calabresi et al., 1997, 1999, 2000; Centonze at al., 2001; Saulle et al., 2004).

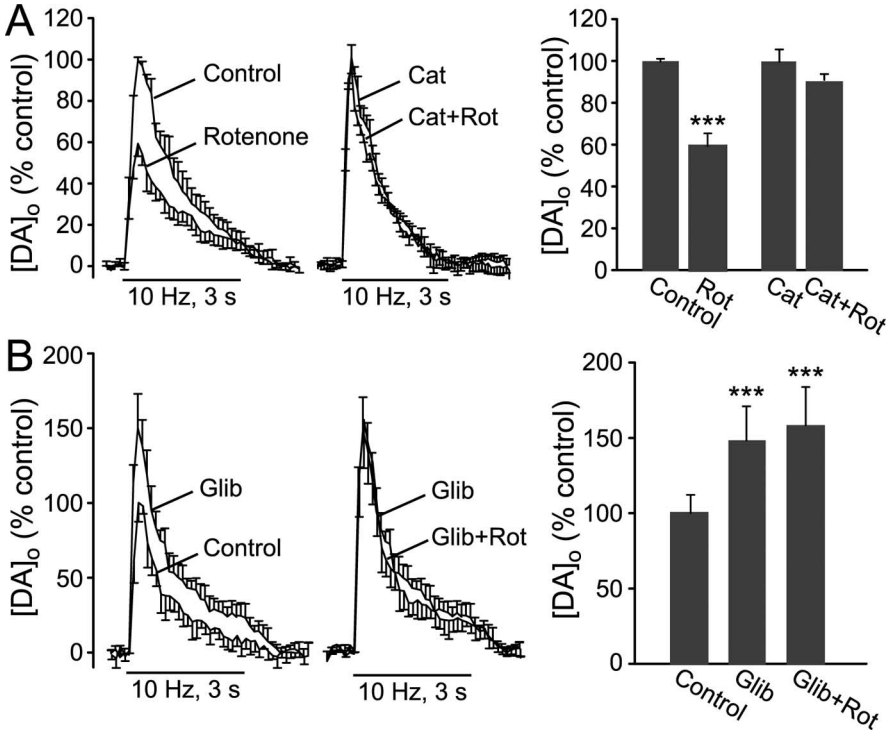

Figure 6. Enhanced suppression of DA release by rotenone with pulse-train stimulation also requires H_2O_2 and K_{ATP} channel opening. ***A***, Average DA release records elicited by 30 pulses (10 Hz) under control conditions (Control) and after 30 min exposure to rotenone (Rot) (50 nM) compared with the effect of rotenone on pulse-train evoked $[DA]_o$ in the presence of catalase (Cat) (500 U/ml). Under control conditions (ACSF alone or ACSF plus heat-inactivated catalase), rotenone caused a significant decrease in peak evoked $[DA]_o$ (***$p < 0.001$ rotenone vs control; $n = 7$); however, this effect of rotenone was prevented in the continued presence of catalase ($p > 0.05$ vs same-site control in catalase alone; $n = 5$). ***B***, Average pulse-train evoked DA release records under control conditions, in the presence of glibenclamide (Glib) (3 μM), and after rotenone in glibenclamide. Glibenclamide caused an increase in pulse-train evoked $[DA]_o$ (***$p < 0.001$ vs control; $n = 5$) and prevented rotenone-induced suppression of DA release ($p > 0.05$ vs glibenclamide alone; ***$p < 0.001$ vs control). Error bars indicate SE.

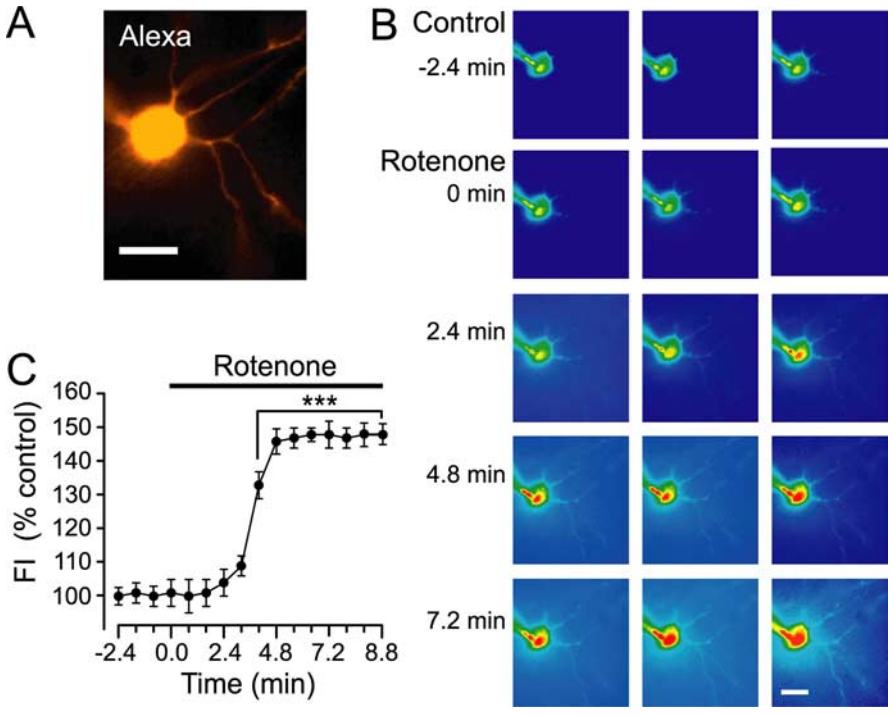

Figure 7. Rotenone increases H_2O_2 generation in striatal medium spiny neurons. ***A***, Medium spiny neuron visualized with Alexa Red during physiological recording *in vitro*. ***B***, DCF fluorescence in the cell in **A** under control conditions and during exposure to rotenone (50 nM). Scale bars: ***A***, ***B***, 20 μm. ***C***, Average time course and amplitude of H_2O_2 generation [DCF fluorescence intensity (FI)] during rotenone exposure ($n = 13$; ***$p < 0.001$ rotenone vs basal FI; ANOVA). Error bars indicate SE.

Most nonselective cation channels are now recognized to be part of the transient receptor potential (TRP) superfamily of cation channels that are activated in response to changes in their local environment (Moran et al., 2004). We therefore examined whether TRP channel opening might underlie rotenone-induced changes in membrane potential and input resistance using the analgesic, flufenamic acid (FFA) (10–100 μM) (Bengtson et al., 2004; Zhu et al., 2005), which is a potent, TRP channel inhibitor (Hill et al., 2004). In pilot studies, we found that 100 μM FFA alone caused a marked depolarization of medium spiny neurons ($n = 3$) and was not tested further. At 10 μM, FFA did not alter resting membrane properties (compare baseline data for control and FFA in Fig. 9*D*,*E*). However, at this concentration, FFA markedly inhibited the effects of 50 nM rotenone on membrane potential (Fig. 9*D*) and input resistance (Fig. 9*E*) ($n = 5$; $p < 0.001$ vs rotenone alone at time points ≥5 min). These data implicate activation of TRP channels in the H_2O_2-dependent effects of rotenone on membrane properties of medium spiny neurons.

Medium spiny neurons also express K_{ATP} channels that are metabolically activated and can serve to attenuate nonselective cation-channel-mediated depolarization in these cells (Calabresi et al., 1999; Centonze et al., 2001). We examined the role of K_{ATP} channels in mediating rotenone-induced changes in membrane properties in medium spiny neurons using 3 μM glibenclamide, which was faster-acting than equally effective 100 nM glibenclamide also tested in studies of evoked DA release. As predicted from previous reports, membrane depolarization in the presence of rotenone (50 nM) was enhanced significantly when K_{ATP} channels were blocked by glibenclamide ($n = 5$; $p < 0.001$ vs rotenone alone at time points ≥4 min) (Fig. 9*D*). Demonstrating a significant role for K_{ATP} channels in rotenone-induced membrane conductance changes, glibenclamide also attenuated the usual decrease in input resistance ($n = 5$; $p < 0.001$ vs rotenone alone at time points ≥4 min) (Fig. 9*E*).

Given this evidence for K_{ATP} channel activation, it was somewhat surprising that we did not see a K_{ATP}-channel-dependent hyperpolarization during rotenone application in the presence of FFA. However, FFA, like other available blockers of TRP channels, has a variety of actions, including interactions with several other cation and anion channels (Hill et al., 2004). Although an interaction of

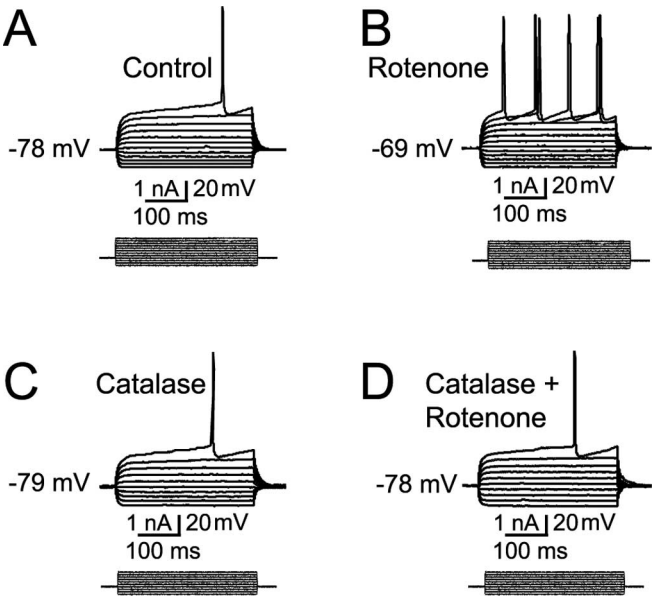

Figure 8. Rotenone alters membrane properties of striatal medium spiny neurons. ***A–D***, Representative current-clamp records during a series of hyperpolarizing and depolarizing current pulses (0.04 nA; 10–12 steps) in medium spiny neurons in striatal slices *in vitro*. ***A***, ***B***, Current-clamp records from the cell shown in Figure 7, *A* and *B*; the pattern of membrane responses under control conditions (***A***) confirmed the identity of the cell as a medium spiny neuron. Rotenone exposure (50 nM; ≤30 min) increased cell excitability ($n = 13$) (***B***), as described in Results. ***C***, ***D***, Current-clamp records from a different medium spiny neuron in the presence of catalase (500 U/ml) and in catalase plus rotenone. In the presence of catalase, rotenone (50 nM; ≤30 min) had no effect on membrane properties in medium spiny neurons ($n = 3$). The usual increase in cell excitability with rotenone was seen in heat-inactivated catalase ($n = 3$); data from heat-inactivated catalase were included in control data averages.

FFA with K_{ATP} channels has not been reported, the nearly complete elimination of rotenone-induced changes in medium spiny neuron membrane properties by FFA would be consistent with concurrent blockade of activated K_{ATP} channels. Consequences of FFA might also include effects on other striatal cells that contribute to the generation of diffusible H_2O_2 and its consequent effects on striatal spiny neuron physiology. We therefore examined the activity dependence of rotenone-induced H_2O_2 generation and consequent effect on medium spiny neuron membrane properties by applying rotenone (50 nM) in the presence of TTX (1 μM). Implicating a role for neuronal activity in the consequences of rotenone exposure, rotenone-enhanced DCF fluorescence was decreased by ~30% in TTX ($n = 3$; $p < 0.05$), accompanied by an attenuation of membrane potential and input resistance changes ~50% ($n = 5$; $p < 0.001$ vs rotenone) (data not shown). Importantly, however, the fact that these changes were not prevented by TTX confirms that a significant contribution is activity independent, implying a direct effect of rotenone on mitochondrial ROS production and its cellular consequences.

Discussion

Here, we report that DA neurotransmission is suppressed in a concentration-dependent manner by nanomolar levels of rotenone known to cause partial inhibition of mitochondrial complex I (Betarbet et al., 2000; Votyakova and Reynolds, 2001). The primary mechanism of DA release inhibition involves rotenone-enhanced H_2O_2 generation and consequent activation of K_{ATP} channels, in the absence of decreased tissue ATP levels. Rotenone-enhanced H_2O_2 generation was confirmed by DCF fluorescence imaging in the principal cells of the striatum, medium spiny neurons, providing the first demonstration of rotenone-dependent ROS generation in intact cells. Simultaneous whole-cell recording revealed that rotenone exposure also caused H_2O_2-dependent membrane depolarization and increased excitability in medium spiny neurons via activation of TRP channels.

These dynamic consequences of mitochondrial inhibition by rotenone were examined in acute brain slices, in which the cellular microenvironment, including local microcircuitry and neuron–glia antioxidant networks, is largely preserved. Previous *in vitro* studies of rotenone toxicity focused on morphological and biochemical changes induced by rotenone, including oxidative damage, cell death, and nigrostriatal degeneration, providing mechanistic insight into rotenone toxicity (Sherer et al., 2003b; Tretter et al., 2004; Testa et al., 2005). However, none of these addressed functional effects of mitochondrial inhibition that might explain the occurrence of profound parkinsonian motor deficits, despite often limited nigrostriatal degeneration after rotenone exposure. This apparent paradox coupled with the additional observation that rotenone is also toxic to non-DA neurons in the basal ganglia (Ferrante et al., 1997; Höglinger et al., 2003; Fleming et al., 2004) have fueled both sides of the debate over the link between exposure to pesticides or other environmental toxicants and Parkinson's disease (Di Monte, 2003; Greenamyre et al., 2003). Importantly, however, Alam and Schmidt (2004) recently reported that rotenone-induced motor deficits can be reversed by L-DOPA, confirming the critical involvement of DA. The present demonstration of striatal DA release inhibition by rotenone provides a unifying explanation for the motor deficits that can accompany rotenone exposure, even when nigrostriatal degeneration is minimal.

DA release suppression by rotenone does not involve ATP depletion

Prevention of rotenone-induced suppression of axonal DA release by the K_{ATP} channel blockers glibenclamide and tolbutamide (Figs. 2, 6*B*) indicates a requirement for K_{ATP} channel opening in release inhibition. Previous studies have shown a role for K_{ATP} channels in regulating DA release in the striatum and DA-neuron activity in the SNc (Avshalumov and Rice, 2003; Avshalumov et al., 2005). Moreover, K_{ATP} channel opening mediates the physiological responses of DA neurons to nanomolar levels of rotenone (Liss et al., 1999). Because intracellular ATP concentration is the primary regulator of K_{ATP} channel opening (Noma, 1983; Cook and Hales, 1984; Ashcroft and Gribble, 1998), we anticipated that the cause of K_{ATP}-channel-dependent inhibition of DA release by rotenone would be ATP depletion. Indeed, from previous studies in isolated mitochondria and synaptosomes (Davey and Clark, 1996; Fonck and Baudry, 2003), 50 nM rotenone would have been predicted to decrease ATP content by as much as 30%. However, using a conventional assay adapted for tissue ATP content, we found that this concentration of rotenone had no effect on ATP levels in the more complex microenvironment of brain slices. Although there was a tendency toward decreased ATP content after 30 min in 50 nM rotenone and a significant depletion in 100 nM rotenone, companion studies in which striatal ATP depletion was induced by lowering media glucose concentration indicated that a ≤15% decrease in ATP content alone was not sufficient

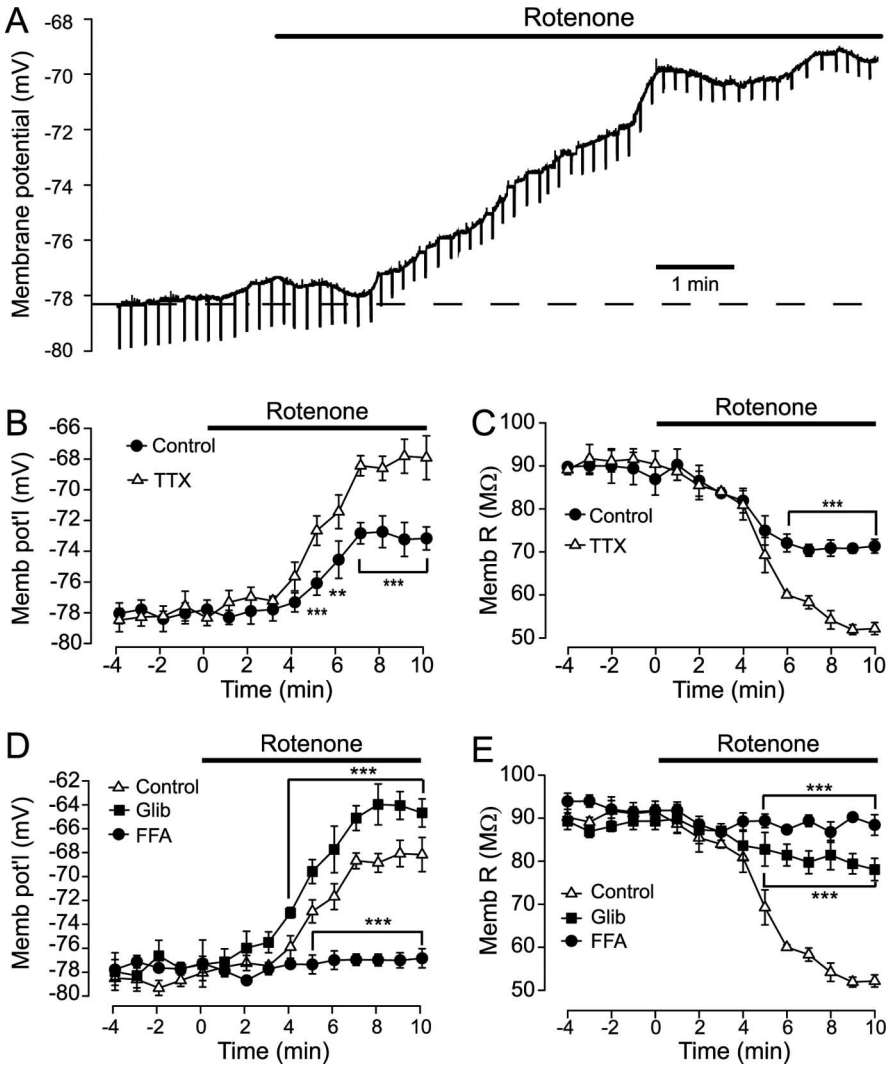

Figure 9. Acute rotenone exposure alters membrane properties of medium spiny neurons. ***A***, Representative current-clamp record showing membrane depolarization in a striatal medium spiny neuron during application of 50 nM rotenone; resting potential in this cell was −78.4 mV (dashed line). Each downward deflection represents the voltage drop produced by pulsed current injection (−0.1 nA; 1 s) used to monitor input resistance during the experiments; the decreasing amplitude of these deflections indicated that a decrease in input resistance accompanied rotenone application. ***B***, Time course of rotenone-induced membrane potential (Memb pot'l) changes in striatal spiny neurons during exposure to 50 nM rotenone ($n = 10$; $^*p < 0.05$; $^{**}p < 0.01$ rotenone vs control; ANOVA). ***C***, Time course of rotenone-induced changes in input resistance (R) for the cells included in ***B*** ($n = 10$; $^{**}p < 0.01$ rotenone vs control; ANOVA). ***D***, Effect of blocking TRP channels with FFA (10 μM) or blocking K_{ATP} channels with glibenclamide (Glib) (3 μM) on rotenone-induced changes in membrane in striatal spiny neurons. Marked suppression of rotenone-induced changes in the presence of FFA implicates activation of TRP channels as the underlying cause of rotenone-induced membrane depolarization in medium spiny neurons ($n = 5$; $^{***}p < 0.001$ vs same time point in 50 nM rotenone alone). Enhanced depolarization in the presence of glibenclamide indicates that activation of K_{ATP} channels during rotenone exposure normally opposes TRP-channel-mediated depolarization ($n = 5$; $^{***}p < 0.001$ vs same time point in 50 nM rotenone alone). ***E***, Effect of FFA ($n = 5$) or glibenclamide ($n = 5$) on rotenone-induced changes in input resistance for the cells included in ***D***; both TRP and K_{ATP} channels contribute to decreased membrane resistance (increased conductance), in the presence of rotenone ($^{***}p < 0.001$ vs same time point in 50 nM rotenone alone). Error bars indicate SE.

to alter DA release (Fig. 4). Together, these data demonstrate that suppression of striatal DA release with nanomolar levels of rotenone is not ATP dependent.

Rotenone-induced DA release suppression requires H_2O_2

What then is the cause of K_{ATP}-channel-dependent DA release inhibition by rotenone? In addition to ATP, another important modulator of K_{ATP} channels is H_2O_2 (Ichinari et al., 1996; Krippeit-Drews et al., 1999; Avshalumov and Rice, 2003; Avshalumov et al., 2003, 2005). In dorsal striatum, modulatory H_2O_2 generated downstream from glutamatergic AMPARs suppresses DA release via K_{ATP} channel activation; this was revealed using local multiple-pulse stimulation, in which concomitantly released glutamate increases H_2O_2 production to cause suppression of DA release evoked by subsequent pulses (Avshalumov et al., 2003). Release of DA elicited by a single stimulus, however, is not modulated by concomitant glutamate release, because the DA release event is over before H_2O_2 generated downstream from AMPARs can act (Avshalumov et al., 2003).

The efficacy of catalase in preventing the K_{ATP}-channel-dependent suppression of single-pulse evoked DA release by 50 nM rotenone, therefore, confirmed an essential role for rotenone-dependent H_2O_2 generation (Fig. 2*D*). In contrast, when pulse-train stimulation was used to elicit DA, rotenone-induced release suppression was exacerbated, suggesting a synergistic amplification of glutamate-dependent H_2O_2 generation during partial mitochondrial inhibition (Fig. 6*A*). Direct confirmation that rotenone caused a functionally relevant increase in H_2O_2 was provided by DCF imaging in individual medium spiny neurons in the absence of local stimulation (Fig. 7*B*,*C*). Although previous studies have shown rotenone-dependent increases in H_2O_2 generation in isolated mitochondria and synaptosomes (Votyakova and Reynolds, 2001; Fonck and Baudry, 2003; Sipos et al., 2003), the present data are the first to demonstrate that rotenone-enhanced H_2O_2 generation is sufficient to overwhelm the relatively intact neuronal and glial antioxidant networks of the complex brain-slice microenvironment.

Importantly, rotenone-enhanced H_2O_2 generation in medium spiny neurons shows that increased ROS levels are not restricted to the nigrostriatal DA pathway. Given that mitochondria are ubiquitous, rotenone-enhanced mitochondrial H_2O_2 generation should occur in all cells and cell processes. The greatest influence on DA release regulation would be expected to come from mitochondria located nearest to DA release sites, including those in DA axons and synapses (Nirenberg et al., 1997), as well as those in dendrites of medium spiny neurons that receive DA synapses (Smith and Bolam, 1990; Avshalumov et al., 2003). However, because H_2O_2 is a neutral, membrane-permeable molecule that can readily diffuse from sites of generation (Ramasarma, 1983; Avshalumov et al., 2003), diffusible H_2O_2 from distant mitochondria could compound local effects. Indeed, attenuation, but not elimination, of

H_2O_2 generation and associated changes in medium spiny neuron membrane properties by TTX implies a significant contribution from tonically active cells and local circuitry, as well as from direct mitochondrial inhibition.

An alternative source of ROS might arise from DA oxidation or metabolism during rotenone exposure. Arguing against this, however, striatal DA and DOPAC contents were unaltered by acute rotenone exposure, indicating maintenance of tissue DA stores and DA turnover under conditions that increased H_2O_2 levels. In addition, peak evoked $[DA]_o$ in the presence of rotenone did not differ from control when K_{ATP} channels were blocked by glibenclamide, showing that DA in the extracellular space is also stable under these conditions.

Rotenone-induced depolarization in medium spiny neurons via TRP channels

Interestingly, although K_{ATP} channels are expressed in medium spiny neurons (Schwanstecher and Panten, 1994; Schwanstecher and Bassen, 1997), rotenone exposure caused membrane depolarization and increased excitability in these cells (Figs. 8*B*, 9). This observation is consistent with previous studies of spiny-neuron physiology under conditions of metabolic stress, including oxygen and/or glucose deprivation or inhibition of mitochondrial complex II, each of which is accompanied by membrane depolarization mediated by nonselective cation channels of the TRP superfamily (Calabresi et al., 1997, 1999, 2000; Centonze at al., 2001; Saulle et al., 2004). Under these conditions, K_{ATP} channels are also activated but serve only to attenuate the predominant TRP-channel-dependent depolarization (Calabresi et al., 1999; Centonze et al., 2001), as seen here (Fig. 9*D*). In contrast, in cholinergic interneurons, another key striatal cell type, rotenone causes profound K_{ATP}-channel-dependent membrane hyperpolarization (Bonsi et al., 2004). Although the high concentrations of rotenone (1–10 μM) examined in those studies would completely inhibit complex I, the opposite responses of cholinergic cells and medium spiny neurons are consistent with response patterns seen with other metabolic challenges (Calabresi et al., 1999; Centonze et al., 2001). The inability of K_{ATP} channels to hyperpolarize striatal spiny neurons and thereby curtail energy consumption has been proposed to contribute to the particular vulnerability of these cells to metabolic stress (Calabresi et al., 1997, 2000; Saulle et al., 2004).

Previous *in vitro* studies have shown that high levels of exogenous H_2O_2 ($\geq$10 mM) can also cause membrane depolarization in medium spiny neurons via TRP channels (Smith et al., 2003); the channel subtype implicated is TRPM2, because other studies indicate that these can be activated by oxidant stress (Perraud et al., 2003; Smith et al., 2003; McNulty and Fonfria, 2005). The studies by Smith et al. (2003), however, did not examine secondary consequences of high levels of exogenous H_2O_2, including ATP depletion that can arise from H_2O_2-dependent inhibition of mitochondrial respiration in a cycle of enhanced ROS production and additional metabolic inhibition (Krippeit-Drews et al., 1999; Fiskum et al., 2003; Kudin et al., 2004; Tretter et al., 2004; Zeevalk et al., 2005). In the present work, rotenone-induced changes in membrane properties occurred in the absence of a change in tissue ATP and were prevented by catalase (Fig. 8*D*), as well as by FFA (Fig. 9*D*,*E*), a TRPM2 channel blocker (Hill et al., 2004), indicating that brain TRP channels, like K_{ATP} channels, are potential targets for regulation by endogenous H_2O_2.

Implications

Parkinson's disease has been linked to chronic mitochondrial dysfunction, which can lead to oxidative stress and further pathology, including nigrostriatal axon damage from DA oxidation in the striatum (Sonsalla et al., 1997; Berman and Hastings, 1999) and eventual retrograde degeneration of DA neurons in the SNc (Sonsalla et al., 1997; Betarbet et al., 2000; Höglinger et al., 2003). The present demonstration of H_2O_2 generation and consequent DA release suppression in the striatum provide new perspectives on the sequelae of pathological events that can accompany mitochondrial dysfunction. Moreover, local effects on striatal DA release would be compounded by concurrent effects on DA-neuron activity in the SNc, because mitochondrial dysfunction (e.g., that induced by nanomolar rotenone) causes K_{ATP}-channel-dependent inhibition of DA-neuron activity (Liss et al., 1999), which would further enhance DA-dependent motor deficits in the absence of frank DA-neuron loss.

References

Alam M, Schmidt WJ (2004) L-DOPA reverses the hypokinetic behaviour and rigidity in rotenone-treated rats. Behav Brain Res 153:439–446.

Ashcroft FM, Gribble FM (1998) Correlating structure and function in ATP-sensitive K^+ channels. Trends Neurosci 21:288–294.

Avshalumov MV, Rice ME (2003) Activation of ATP-sensitive K^+ (K_{ATP}) channels by H_2O_2 underlies glutamate-dependent inhibition of striatal dopamine release. Proc Natl Acad Sci USA 100:11729–11734.

Avshalumov MV, Chen BT, Marshall SP, Peña DM, Rice ME (2003) Glutamate-dependent inhibition of dopamine release in striatum is mediated by a new diffusible messenger, H_2O_2. J Neurosci 23:2744–2750.

Avshalumov MV, Chen BT, Koós T, Tepper JM, Rice ME (2005) Endogenous hydrogen peroxide regulates the excitability of midbrain dopamine neurons via ATP-sensitive channels. J Neurosci 25:4222–4231.

Bengtson CP, Tozzi A, Bernardi G, Mercuri NB (2004) Transient receptor potential-like channels mediate metabotropic glutamate receptor EPSCs in rat dopamine neurones. J Physiol (Lond) 555:323–330.

Berman SB, Hastings TG (1999) Dopamine oxidation alters mitochondrial respiration and induces permeability transition in brain mitochondria: implications for Parkinson's disease. J Neurochem 73:1127–1137.

Betarbet R, Sherer TB, MacKenzie G, Garcia-Osuna M, Panov AV, Greenamyre JT (2000) Chronic systemic pesticide exposure reproduces features of Parkinson's disease. Nat Neurosci 3:1301–1306.

Bonsi P, Calabresi P, De Persis C, Papa M, Centonze D, Bernardi G, Pisani A (2004) Early ionic and membrane potential changes caused by the pesticide rotenone in striatal cholinergic interneurons. Exp Neurol 185:169–181.

Calabresi P, Ascone CM, Centonze D, Pisani A, Sancesario G, D'Angelo V, Bernardi G (1997) Opposite membrane potential changes induced by glucose deprivation in striatal spiny neurons and in large aspiny interneurons. J Neurosci 17:1940–1949.

Calabresi P, Marfia GA, Centonze D, Pisani A, Bernardi G (1999) Sodium influx plays a major role in the membrane depolarization induced by oxygen and glucose deprivation in rat striatal spiny neurons. Stroke 30:171–179.

Calabresi P, Centonze D, Bernardi G (2000) Cellular factors controlling neuronal vulnerability in the brain: a lesson from the striatum. Neurology 55:1249–1255.

Centonze D, Marfia GA, Pisani A, Picconi B, Giacomini P, Bernardi G, Calabresi P (2001) Ionic mechanisms underlying differential vulnerability to ischemia in striatal neurons. Prog Neurobiol 63:687–696.

Chen BT, Avshalumov MV, Rice ME (2001) H_2O_2 is a novel, endogenous modulator of synaptic dopamine release. J Neurophysiol 85:2468–2476.

Cook DL, Hales CN (1984) Intracellular ATP directly blocks K^+ channels in pancreatic β-cells. Nature 311:271–273.

Cragg SJ (2003) Variable dopamine release probability and short-term plasticity between functional domains of the primate striatum. J Neurosci 23:4378–4385.

Crepel V, Krnjevic K, Ben-Ari Y (1993) Sulphonylureas reduce the slowly

inactivating D-type outward current in rat hippocampal neurons. J Physiol (Lond) 466:39–54.
Dauer W, Przedborski S (2003) Parkinson's disease: mechanisms and models. Neuron 39:889–909.
Davey GP, Clark JB (1996) Threshold effects and control of oxidative phosphorylation in nonsynaptic rat brain mitochondria. J Neurochem 66:1617–1624.
Dawson TM, Dawson VL (2003) Molecular pathways of neurodegeneration in Parkinson's disease. Science 302:819–822.
Di Monte DA (2003) The environment and Parkinson's disease: is the nigrostriatal system preferentially targeted by neurotoxins? Lancet Neurol 2:531–538.
Ferrante RJ, Schulz JB, Kowall NW, Beal MF (1997) Systemic administration of rotenone produces selective damage in the striatum and globus pallidus, but not in the substantia nigra. Brain Res 753:157–162.
Fiskum G, Starkov A, Polster BM, Chinopoulos C (2003) Mitochondrial mechanisms of neural cell death and neuroprotective interventions in Parkinson's disease. Ann NY Acad Sci 991:111–119.
Fleming SM, Zhu C, Fernagut PO, Mehta A, DiCarlo CD, Seaman RL, Chesselet MF (2004) Behavioral and immunohistochemical effects of chronic intravenous and subcutaneous infusions of varying doses of rotenone. Exp Neurol 187:418–429.
Fonck C, Baudry M (2003) Rapid reduction of ATP synthesis and lack of free radical formation by MPP^+ in rat brain synaptosomes and mitochondria. Brain Res 975:214–221.
Greenamyre JT, Sherer TB, Betarbet R, Panov AV (2001) Complex I and Parkinson's disease. IUBMB Life 52:135–141.
Greenamyre JT, Betarbet R, Sherer TB (2003) The rotenone model of Parkinson's disease: genes, environment and mitochondria. Parkinsonism Relat Disord 9 [Suppl 2]:S59–S64.
Gyulkhandanyan AV, Pennefather PS (2004) Shift in the localization of sites of hydrogen peroxide production in brain mitochondria by mitochondrial stress. J Neurochem 90:405–421.
Hill K, Benham CD, McNulty S, Randall AD (2004) Flufenamic acid is a pH-dependent antagonist of TRPM2 channels. Neuropharmacology 47:450–460.
Höglinger GU, Feger J, Prigent A, Michel PP, Parain K, Champy P, Ruberg M, Oertel WH, Hirsch EC (2003) Chronic systemic complex I inhibition induces a hypokinetic multisystem degeneration in rats. J Neurochem 84:491–502.
Ichinari K, Kakei M, Matsuoka T, Nakashima H, Tanaka H (1996) Direct activation of the ATP-sensitive potassium channel by oxygen free radicals in guinea-pig ventricular cells: its potentiation by MgADP. J Mol Cell Cardiol 28:1867–1877.
Kemp JM, Powell TP (1971) The structure of the caudate nucleus of the cat: light and electron microscopy. Philos Trans R Soc Lond B Biol Sci 262:383–401.
Koós T, Tepper JM (1999) Inhibitory control of neostriatal projection neurons by GABAergic interneurons. Nat Neurosci 2:467–472.
Krippeit-Drews P, Kramer C, Welker S, Lang F, Ammon HPT, Drews G (1999) Interference of H_2O_2 with stimulus-secretion coupling in mouse pancreatic β-cells. J Physiol (Lond) 514:471–481.
Kudin AP, Bimpong-Buta NY, Vielhaber S, Elger CE, Kunz WS (2004) Characterization of superoxide-producing sites in isolated brain mitochondria. J Biol Chem 279:4127–4135.
Kwong LK, Sohal RS (1998) Substrate and site specificity of hydrogen peroxide generation in mouse mitochondria. Arch Biochem Biophys 350:118–126.
Liss B, Bruns R, Roeper J (1999) Alternative sulfonylurea receptor expression defines sensitivity to K-ATP channels in dopaminergic midbrain neurons. EMBO J 18:833–846.
McNulty S, Fonfria E (2005) The role of TRPM channels in cell death. Pflügers Arch, in press.
Moran MM, Xu H, Clapham DE (2004) TRP ion channels in the nervous system. Curr Opin Neurobiol 14:362–369.
Nirenberg MJ, Chan J, Liu Y, Edwards RH, Pickel VM (1997) Vesicular monoamine transporter-2: immunogold localization in striatal axons and terminals. Synapse 26:194–198.
Nisenbaum ES, Wilson CJ (1995) Potassium currents responsible for inward and outward rectification in rat neostriatal spiny projection neurons. J Neurosci 15:4449–4463.
Noma A (1983) ATP-regulated K^+ channels in cardiac muscle. Nature 305:147–148.
Olanow CW, Tatton WG (1999) Etiology and pathogenesis of Parkinson's disease. Annu Rev Neurosci 22:123–144.
Orth M, Schapira AH (2002) Mitochondrial involvement in Parkinson's disease. Neurochem Int 40:533–541.
Parker Jr WD, Boyson SJ, Parks JK (1989) Abnormalities of the electron transport chain in idiopathic Parkinson's disease. Ann Neurol 26:719–723.
Perraud AL, Schmitz C, Scharenberg AM (2003) TRPM2 Ca^{2+} permeable cation channels: from gene to biological function. Cell Calcium 33:519–531.
Ramasarma T (1983) Generation of H_2O_2 in biomembranes. Biochem Biophys Acta 694:69–93.
Reynolds IJ, Hastings TG (1995) Glutamate induces the production of reactive oxygen species in cultured forebrain neurons following NMDA receptor activation. J Neurosci 15:3318–3327.
Rice ME, Cragg SJ (2004) Nicotine amplifies reward-related dopamine signals in striatum. Nat Neurosci 7:583–584.
Rice ME, Nicholson C (1991) Diffusion characteristics and extracellular volume fraction during normoxia and hypoxia in slices of rat neostriatum. J Neurophysiol 65:264–272.
Rice ME, Russo-Menna I (1998) Differential compartmentalization of brain ascorbate and glutathione between neurons and glia. Neuroscience 82:1213–1223.
Sah R, Schwartz-Bloom RD (1999) Optical imaging reveals elevated intracellular chloride in hippocampal pyramidal cells after oxidative stress. J Neurosci 19:9209–9217.
Saulle E, Gubellini P, Picconi B, Centonze D, Tropepi D, Pisani A, Morari M, Marti M, Rossi L, Papa M, Bernardi G, Calabresi P (2004) Neuronal vulnerability following inhibition of mitochondrial complex II: a possible ionic mechanism for Huntington's disease. Mol Cell Neurosci 25:9–20.
Schaffer P, Pelzmann B, Bernhart E, Lang P, Machler H, Rigler B, Koidl B (1999) The sulphonylurea glibenclamide inhibits voltage dependent potassium currents in human atrial and ventricular myocytes. Br J Pharmacol 128:1175–1180.
Schapira AH, Cooper JM, Dexter D, Clark JB, Jenner P, Marsden CD (1990) Mitochondrial complex I deficiency in Parkinson's disease. J Neurochem 54:823–827.
Schwanstecher C, Bassen D (1997) K_{ATP}-channel on the somata of spiny neurones in rat caudate nucleus: regulation by drugs and nucleotides. Br J Pharmacol 121:193–198.
Schwanstecher C, Panten U (1994) Identification of an ATP-sensitive K^+ channel in spiny neurons of rat caudate nucleus. Pflügers Arch 427:187–189.
Sherer TB, Kim JH, Betarbet R, Greenamyre JT (2003a) Subcutaneous rotenone exposure causes highly selective dopaminergic degeneration and alpha-synuclein aggregation. Exp Neurol 179:9–16.
Sherer TB, Betarbet R, Testa CM, Seo BB, Richardson JR, Kim JH, Miller GW, Yagi T, Matsuno-Yagi A, Greenamyre JT (2003b) Mechanism of toxicity in rotenone models of Parkinson's disease. J Neurosci 23:10756–10764.
Sipos I, Tretter L, Adam-Vizi V (2003) Quantitative relationship between inhibition of respiratory complexes and formation of reactive oxygen species in isolated nerve terminals. J Neurochem 84:112–118.
Smith AD, Bolam JP (1990) The neural network of the basal ganglia as revealed by the study of synaptic connections of identified neurons. Trends Neurosci 13:259–265.
Smith MA, Herson PS, Lee K, Pinnock RD, Ashford ML (2003) Hydrogen-peroxide-induced toxicity of rat striatal neurones involves activation of a non-selective cation channel. J Physiol (Lond) 547:417–425.
Sonsalla PK, Manzino L, Sinton CM, Liang CL, German DC, Zeevalk GD (1997) Inhibition of striatal energy metabolism produces cell loss in the ipsilateral substantia nigra. Brain Res 773:223–226.
Testa CM, Sherer TB, Greenamyre JT (2005) Rotenone induces oxidative stress and dopaminergic neuron damage in organotypic substantia nigra cultures. Mol Brain Res 134:109–118.

Tretter L, Sipos I, Adam-Vizi V (2004) Initiation of neuronal damage by complex I deficiency and oxidative stress in Parkinson's disease. Neurochem Res 29:569–577.

Valente EM, Abou-Sleiman PM, Caputo V, Muqit MM, Harvey K, Gispert S, Ali Z, Del Turco D, Bentivoglio AR, Healy DG, Albanese A, Nussbaum R, Gonzalez-Maldonado R, Deller T, Salvi S, Cortelli P, Gilks WP, Latchman DS, Harvey RJ, Dallapiccola B, et al. (2004) Hereditary early-onset Parkinson's disease caused by mutations in PINK1. Science 304:1158–1160.

Votyakova TV, Reynolds IJ (2001) $\Delta\Psi_m$-Dependent and -independent production of reactive oxygen species by rat brain mitochondria. J Neurochem 79:266–277.

Witkovsky P, Nicholson C, Rice ME, Bohmaker K, Meller E (1993) Extracellular dopamine concentration in the retina of the clawed frog, *Xenopus laevis*. Proc Natl Acad Sci USA 90:5667–5671.

Zeevalk GD, Bernard LP, Song C, Gluck M, Ehrhart J (2005) Mitochondrial inhibition and oxidative stress: reciprocating players in neurodegeneration. Antioxid Redox Signal 7:1117–1139.

Zhang Y, Dawson VL, Dawson TM (2000) Oxidative stress and genetics in the pathogenesis of Parkinson's disease. Neurobiol Dis 7:240–250.

Zhu ZT, Munhall A, Shen KZ, Johnson SW (2005) NMDA enhances a depolarization-activated inward current in subthalamic neurons. Neuropharmacology 49:317–327.

Zigmond MJ, Abercrombie ED, Berger TW, Grace AA, Stricker EM (1990) Compensations after lesions of central dopaminergic neurons: some clinical and basic implications. Trends Neurosci 13:290–296.